Available online at www.sciencedirect.com
SCIENCE DIRECT®
Journal of Solid State Chemistry 172 (2003) 6–11
JOURNAL OF SOLID STATE CHEMISTRY
http://elsevier.com/locate/jssc

Synthesis and characterization of two-dimensional fluorinated metal phosphates incorporating 2,2′-bipyridine ligands: $M_2F_2(2,2'\text{-bpy})(HPO_4)_2(H_2O)$ (M = Fe, Ga)

Wen-Jung Chang,[a] Chun-Yu Chen,[a] and Kwang-Hwa Lii[a,b,*]

[a] Department of Chemistry, National Central University, Chungli, Taiwan, ROC
[b] Institute of Chemistry, Academia Sinica, Nankang, Taipei, Taiwan, ROC

Received 27 September 2002; accepted 5 January 2003

Abstract

Two fluorinated metal phosphates, $M_2F_2(2,2'\text{-bpy})(HPO_4)_2(H_2O)$ (M = Fe, Ga), have been synthesized under hydrothermal conditions and characterized by single-crystal X-ray diffraction, thermogravimetric analysis, and magnetic susceptibility. The two compounds are isostructural and crystallize in the triclinic space group $p\bar{1}$, $a = 7.6595(8)$ Å, $b = 10.101(1)$ Å, $c = 11.260(1)$ Å, $\alpha = 107.555(2)^\circ$, $\beta = 105.174(2)^\circ$, $\gamma = 98.975(2)^\circ$, $V = 775.1(2)$ Å^3 and $Z = 2$ for the Fe compound, and $a = 7.5816(6)$ Å, $b = 9.9943(7)$ Å, $c = 11.1742(8)$ Å, $\alpha = 107.333(1)^\circ$, $\beta = 105.014(1)^\circ$, $\gamma = 99.261(1)^\circ$ and $V = 754.2(2)$ Å^3 for the Ga compound. They are the first fluorinated metal phosphates which incorporate 2,2′-bipyridine ligands. The structure consists of edge-sharing octahedral dimers with the composition $Fe_2F_4(H_2O)_2O_4$ and discrete FeN_2O_4 octahedra, which are linked into two-dimensional sheets through corner-sharing phosphate tetrahedra. The 2,2′-bpy ligands bind in a bidentate fashion to the metal atoms and project into interlamellar region. The layers are extended into a three-dimensional supramolecular array via $\pi-\pi$ stacking interactions of the 2,2′-bpy ligands. Magnetic susceptibility of the iron compound confirms the presence of Fe^{III}.

1. Introduction

Recently, many research activities have focused on the synthesis of new open-framework metal phosphates, owing to their diverse structural chemistry and potential applications [1–3]. In the context of building open-frameworks, it is also possible to use organic molecules in the skeleton. As compared with inorganic phosphates, the organic molecules have larger sizes of polyhedral centers and a wide variety of means of connection. The organic components can greatly affect the connecting patterns of inorganic polyhedra, thus providing a method for the synthesis of new materials. An interesting variant of the metal phosphates is obtained by incorporating oxalate unit in the structures. A good number of oxalatophosphates of transition metals and Group 13 elements have been reported during the past few years [4–17]. Most of these compounds consist of anionic 3-D frameworks templated with organic amines in protonated forms, while a few contain neutral frameworks without organic amine templates. Three types of oxalate coordination are observed in these structures, namely, bisbidentate, monobidentate, and bismono- and bisbidentate. Another class of organic–inorganic hybrid compounds is based on 4,4′-bipyridine and phosphate, in which the metal cations are coordinated by both types of ligands [18–24]. In these structures the 4,4′-bpy unit can act as a monoprotonated pendant ligand or as a neutral bridging ligand. About a half of the reported structures in this system consist of metal phosphate layers pillared by 4,4′-bpy ligands. This structure type exhibits the characteristic pattern of alternating organic-inorganic domains often observed in metal organophosphonate phases [25]. Recently we were interested in using 2,2′-bipyridine or 1,10-phenanthroline to synthesize new organic–inorganic hybrid compounds, and have now isolated several new phases in the 2,2′-bpy-phosphate system. In this work we report the synthesis and characterization of a fluorinated iron phosphate $Fe_2F_2(2,2'\text{-bpy})(HPO_4)_2(H_2O)$ (**1**) and the

*Corresponding author. Department of Chemistry, National Central University, Chungli, Taiwan, ROC. Fax: +886-3-422-7664.
E-mail address: liikh@cc.ncu.edu.tw (K.-H. Lii).

0022-4596/03/$ - see front matter © 2003 Elsevier Science (USA). All rights reserved.
doi:10.1016/S0022-4596(03)00083-5

gallium analogue $Ga_2F_2(2,2'\text{-bpy})(HPO_4)_2(H_2O)$ (**2**). They are the first fluorinated metal phosphates which incorporate 2,2′-bipyridine ligands.

2. Experimental section

2.1. Synthesis and initial characterization

The hydrothermal reactions were carried out in Teflon-lined stainless steel Parr acid digestion bombs. All chemicals were purchased from Aldrich. A reaction mixture of $FeCl_3 \cdot 6H_2O$ (2 mmol), 2,2′-bipyridine (1 mmol), H_3PO_4 (2 mmol), hydrofluoric acid (2 mmol) and H_2O (10 mL) was heated at 180°C for 3 days followed by slow cooling to room temperature at 10°C/h. The solid product was filtered off, washed with water, rinsed with ethanol and dried in a desiccator at room temperature to give yellow–green columnar crystals of **1** in 77% yield based on Fe. A suitable crystal was selected for structure determination by single-crystal X-ray diffraction. The product was monophasic because its powder X-ray diffraction pattern was in good agreement with the calculated pattern based on the atomic coordinates derived from single-crystal X-ray diffraction (Fig. 1). However, the intensities of 0 0 *l* reflections were considerably greater than the values simulated from single-crystal data because of preferred orientation of crystals within the powder specimen. EDX and EPMA analyses of several crystals showed the presence of Fe, P, and F elements. Elemental analysis confirmed its stoichiometry. Anal. Found: C, 23.32%; H, 2.37%; N, 5.32%. Calc.: C, 23.28%; H, 2.34%; N, 5.43%. The gallium compound, **2**, was obtained in a yield of 78% by reacting $Ga(NO_3)_3 \cdot 4H_2O$ (2 mmol), 2,2′-bipyridine (2 mmol), H_3PO_4 (3 mmol), hydrofluoric acid (2 mmol) and H_2O (10 mL) under the same reaction conditions. The bulk product was monophasic as indicated by powder X-ray diffraction.

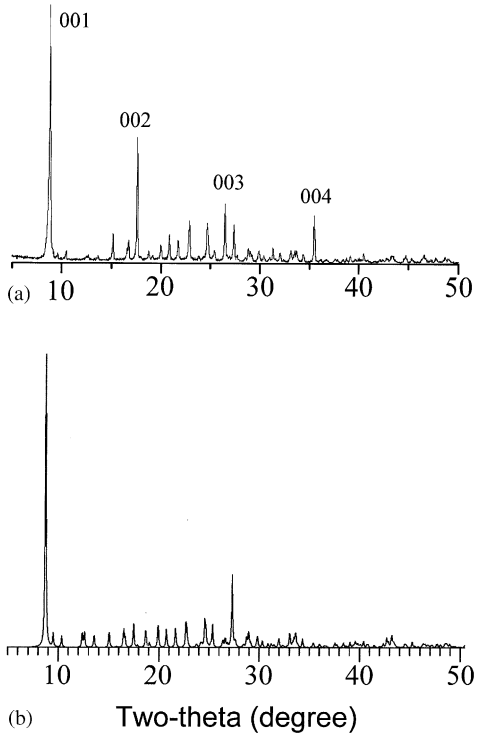

Fig. 1. (a) X-ray powder pattern of **1**. (b) Simulated powder pattern from the atomic coordinates derived from single-crystal X-ray diffraction.

2.2. TGA and magnetic susceptibility measurements

Thermogravimetric analysis of **1** was performed on a Perkin-Elmer TGA 7 thermal analyzer; the sample was heated in flowing oxygen from 40°C to 600°C at 10°C/min and then the rate was changed to 5°C/min from 600°C to 900°C. Variable-temperature magnetic susceptibility $\chi(T)$ data were obtained on 40.0 mg of polycrystalline sample of **1** from 2 to 300 K in a magnetic field of 5000 G after zero-field cooling using a SQUID magnetometer. Correction for diamagnetism was made according to Kahn [26].

2.3. Single-crystal X-ray diffraction

A suitable single crystal of each compound was selected for indexing and intensity data collection on a Siemens Smart-CCD diffractometer equipped with a normal focus, 3 kW sealed tube X-ray source at room temperature. Empirical absorption corrections based on symmetry equivalents were applied. The structures were solved by direct methods and subsequent difference Fourier syntheses. Bond-valence calculations indicate that O(4) and O(8) are hydroxo oxygen atoms, and O(9) is a water oxygen atom [27]. There are two HPO_4 groups and one water molecule in an asymmetric unit. The hydrogen atoms bonded to oxygen atoms were located in difference maps. The hydrogen atoms, which are bonded to carbon atoms, were positioned geometrically and refined using a riding model with fixed isotropic thermal parameters. To balance charge the atoms which connect neighboring metal atoms or coordinate to the metal atoms as terminal ligands are fluorine atoms. The terminal *M*–F bond is significantly shorter than *M*–OH_2. There are two F atoms per asymmetric unit. The final cycles of least-squares refinement included atomic coordinates and anisotropic thermal parameters for all non-hydrogen atoms. The reliability factors converged to $R1 = 0.0485$, $wR2 = 0.0913$, and $S = 0.973$ for **1** and $R1 = 0.0253$, $wR2 = 0.0705$, and $S = 1.104$ for **2**. All calculations were performed using the SHEXTL Version 5.1 software package [28]. The crystallographic data is given in Table 1, atomic coordinates in Table 2, and selected bond distances in Table 3.

Table 1
Crystallographic data for $Fe_2F_2(2,2'\text{-bpy})(HPO_4)_2(H_2O)$ (**1**) and $Ga_2F_2(2,2'\text{-bpy})(HPO_4)_2(H_2O)$ (**2**)

	1	**2**
Crystal size (mm)	$0.15\times0.1\times0.07$	$0.15\times0.06\times0.03$
Crystal system	Triclinic	Triclinic
Space group	$p\bar{1}$ (No. 2)	$p\bar{1}$ (No. 2)
A (Å)	7.6595(8)	7.5816(6)
B (Å)	10.101(1)	9.9943(7)
c (Å)	11.260(1)	11.1742(8)
α (deg)	107.555(2)	107.333(1)
β (deg)	105.174(2)	105.014(1)
γ (deg)	98.975(2)	99.261(1)
V (Å)^3	775.1(2)	754.2(2)
Z	2	2
f_w	515.86	543.60
T (K)	296	296
λ (Mo$K\alpha$) (Å)	0.71073	0.71073
ρ_{calc} (g cm^{-3})	2.210	2.394
μ(Mo$K\alpha$) (cm^{-1})	21.6	38.7
$T_{min,\,max}$	0.907/0.974	0.768, 0.962
$2\theta_{max}$ (deg)	56.6	56.6
Unique data ($I>2\sigma(I)$)	2465	2929
No. of variables	244	244
R_1[a]	0.0485	0.0253
wR_2[b]	0.0913	0.0705
$(\Delta\rho)_{max,\,min}$	1.14, −0.39	0.60, −0.56

[a] $R_1=\sum||F_o|-F_c||/\sum|F_o|$.

[b] $wR_2=\sum[w(F_o^2-F_c^2]/\sum[w(F_o^2)^2]^{1/2}$, $w=1/[\sigma^2(F_o)+(aP)^2+bP]$, $P=[\mathrm{Max}(F_o,0)+2(F_c)^2]/3$, where $a=0.0356$ and $b=0$ for **1** and $a=0.0369$ and $b=0.18$ for **2**.

3. Results and discussion

3.1. TGA and magnetic susceptibility

The TGA curve shows a broad weight loss in several overlapping steps, which begins gradually at ca. 100°C and is complete at ca. 800°C (Fig. 2). The final decomposition product is $FePO_4$ (JCPDS: 29–715), as indicated from powder X-ray diffraction. The total weight loss between 40°C and 900°C is 42.6% which is close to the calculated value of 41.5% according to the following equation.

$$Fe_2F_2(2,2'\text{-bpy})(HPO_4)_2(H_2O) \rightarrow 2FePO_4+C_{10}H_8N_2+2HF+H_2O.$$

As shown in Fig. 3, the $\chi_M T$ value decreases with decreasing temperature, indicating that the main magnetic interactions between Fe atoms are antiferromagnetic. The effective magnetic moment at 300 K is $2.83(\chi_M T/2)^{1/2}=5.75\,\mu_B$/Fe as compared with the value of 5.92 μ_B/Fe expected for spin-only and non-interacting Fe^{3+} ions. The inverse magnetic susceptibility follows the Curie–Weiss law in the paramagnetic state (for $T>25$ K), and the Weiss temperature θ_P is strongly negative (−47.7 K), which is consistent with antiferromagnetic interactions.

Table 2
Atomic coordinates and thermal parameters for $Fe_2F_2(2,2'\text{-bpy})(HPO_4)_2(H_2O)$ (**1**) and $Ga_2F_2(2,2'\text{-bpy})(HPO_4)_2(H_2O)$ (**2**)[a]

Atom	x	y	z	U_{eq} (Å^2)[b]
Compound **1**				
Fe(1)	0.19246(8)	0.56538(6)	0.48827(6)	0.0130(2)
Fe(2)	−0.34968(8)	0.90558(6)	0.35380(6)	0.0113(2)
P(1)	0.0486(2)	0.8073(1)	0.3831(1)	0.0113(2)
P(2)	−0.4506(2)	0.8359(1)	0.5947(1)	0.0116(2)
F(1)	0.0253(3)	0.6066(2)	0.5957(2)	0.0188(6)
F(2)	0.3136(3)	0.4693(2)	0.3736(2)	0.0196(6)
O(1)	0.0865(4)	0.6623(3)	0.3753(3)	0.0159(7)
O(2)	−0.1605(4)	0.7916(3)	0.3596(3)	0.0154(7)
O(3)	0.1720(4)	0.9253(3)	0.5107(3)	0.0168(7)
O(4)	0.0881(4)	0.8424(3)	0.2642(3)	0.0196(7)
O(5)	−0.6065(4)	0.7303(3)	0.6039(3)	0.0157(7)
O(6)	−0.4617(4)	0.8100(3)	0.4528(3)	0.0163(7)
O(7)	−0.4419(4)	0.9918(3)	0.6692(3)	0.0140(6)
O(8)	−0.2609(4)	0.8126(3)	0.6703(3)	0.0189(7)
O(9)	0.3169(4)	0.4677(3)	0.6157(3)	0.0197(7)
N(1)	−0.5314(5)	0.7321(4)	0.1738(4)	0.0157(8)
N(2)	−0.2890(5)	0.9590(4)	0.1956(4)	0.0158(8)
C(1)	−0.6558(6)	0.6205(5)	0.1703(5)	0.021(1)
C(2)	−0.7655(7)	0.5109(5)	0.0546(5)	0.030(1)
C(3)	−0.7487(8)	0.5181(6)	−0.0627(6)	0.036(1)
C(4)	−0.6250(7)	0.6327(5)	−0.0615(5)	0.030(1)
C(5)	−0.5154(6)	0.7377(5)	0.0584(4)	0.018(1)
C(6)	−0.3778(6)	0.8662(5)	0.0716(4)	0.017(1)
C(7)	−0.3446(7)	0.8929(6)	−0.0345(5)	0.029(1)
C(8)	−0.2205(7)	1.0190(6)	−0.0136(5)	0.033(1)
C(9)	−0.1330(7)	1.1134(6)	0.1121(5)	0.029(1)
C(10)	−0.1676(6)	1.0809(5)	0.2165(5)	0.019(1)
Compound **2**				
Ga(1)	0.19266(4)	0.56596(3)	0.49080(3)	0.01258(9)
Ga(2)	−0.35071(4)	0.90286(3)	0.35070(3)	0.01105(9)
P(1)	0.0489(1)	0.80734(7)	0.38601(7)	0.0112(2)
P(2)	−0.4531(1)	0.83722(8)	0.59427(7)	0.0121(2)
F(1)	0.0238(2)	0.6050(2)	0.5952(2)	0.0171(4)
F(2)	0.3142(2)	0.4724(2)	0.3777(2)	0.0194(4)
O(1)	0.0848(3)	0.6592(2)	0.3767(2)	0.0149(4)
O(2)	−0.1628(3)	0.7898(2)	0.3631(2)	0.0148(4)
O(3)	0.1738(3)	0.9271(2)	0.5127(2)	0.0164(4)
O(4)	0.0867(3)	0.8417(2)	0.2647(2)	0.0196(4)
O(5)	−0.6090(3)	0.7310(2)	0.6055(2)	0.0156(4)
O(6)	−0.4643(3)	0.8115(2)	0.4510(2)	0.0156(4)
O(7)	−0.4434(3)	0.9951(2)	0.6713(2)	0.0136(4)
O(8)	−0.2607(3)	0.8140(2)	0.6700(2)	0.0200(4)
O(9)	0.3133(3)	0.4695(2)	0.6154(2)	0.0183(4)
N(1)	−0.5300(3)	0.7312(2)	0.1771(2)	0.0153(5)
N(2)	−0.2840(3)	0.9602(3)	0.2004(2)	0.0156(5)
C(1)	−0.6565(4)	0.6178(3)	0.1742(3)	0.0200(6)
C(2)	−0.7672(5)	0.5077(4)	0.0572(3)	0.0299(8)
C(3)	−0.7527(5)	0.5150(4)	−0.0614(3)	0.0363(9)
C(4)	−0.6250(5)	0.6321(4)	−0.0591(3)	0.0295(8)
C(5)	−0.5138(4)	0.7375(3)	0.0619(3)	0.0187(6)
C(6)	−0.3738(4)	0.8672(3)	0.0751(3)	0.0191(6)
C(7)	−0.3403(5)	0.8953(4)	−0.0323(3)	0.0285(8)
C(8)	−0.2149(5)	1.0245(4)	−0.0099(3)	0.0321(8)
C(9)	−0.1261(5)	1.1197(4)	0.1182(3)	0.0284(7)
C(10)	−0.1618(4)	1.0836(3)	0.2213(3)	0.0208(6)

[a] The atomic coordinates of hydrogen atoms are given in supplementary materials.

[b] U_{eq} is defined as one third of the trace of the orthogonalized U_{ij} tensor.

Table 3
Bond lengths (Å) for $Fe_2F_2(2,2'\text{-bpy})(HPO_4)_2(H_2O)$ (**1**) and $Ga_2F_2(2,2'\text{-bpy})(HPO_4)_2(H_2O)$ (**2**)[a]

Compound **1**			
Fe(1)–F(1)	1.987(2)	Fe(1)–F(1)#1	1.993(2)[b]
Fe(1)–F(2)	1.904(2)	Fe(1)–O(1)	1.922(3)
Fe(1)–O(5)#2	1.919(3)	Fe(1)–O(9)	2.091(3)
Fe(2)–O(2)	1.987(3)	Fe(2)–O(3)#3	1.927(3)
Fe(2)–O(6)	1.950(3)	Fe(2)–O(7)#4	2.038(3)
Fe(2)–N(1)	2.176(4)	Fe(2)–N(2)	2.148(3)
P(1)–O(1)	1.518(3)	P(1)–O(2)	1.528(3)
P(1)–O(3)	1.511(3)	P(1)–O(4)	1.573(3)
P(2)–O(5)	1.519(3)	P(2)–O(6)	1.516(3)
P(2)–O(7)	1.525(3)	P(2)–O(8)	1.573(3)
N(1)–C(1)	1.341(5)	N(1)–C(5)	1.353(5)
N(2)–C(6)	1.343(5)	N(2)–C(10)	1.337(5)
C(1)–C(2)	1.376(6)	C(2)–C(3)	1.383(7)
C(3)–C(4)	1.370(7)	C(4)–C(5)	1.385(6)
C(5)–C(6)	1.481(6)	C(6)–C(7)	1.377(6)
C(7)–C(8)	1.381(7)	C(8)–C(9)	1.360(7)
C(9)–C(10)	1.390(6)	O(4)–H(4O)	0.958
O(8)–H(8O)	0.895	O(9)–H(9A)	0.767
O(9)–H(9B)	0.899		
Compound **2**			
Ga(1)–F(1)	1.953(2)	Ga(1)–F(1)#1	1.959(2)[b]
Ga(1)–F(2)	1.871(2)	Ga(1)–O(1)	1.891(2)
Ga(1)–O(5)#2	1.889(2)	Ga(1)–O(9)	2.031(2)
Ga(2)–O(2)	1.958(2)	Ga(2)–O(3)#3	1.918(2)
Ga(2)–O(6)	1.920(2)	Ga(2)–O(7)#4	2.000(2)
Ga(2)–N(1)	2.111(2)	Ga(2)–N(2)	2.079(2)
P(1)–O(1)	1.526(2)	P(1)–O(2)	1.530(2)
P(1)–O(3)	1.505(2)	P(1)–O(4)	1.576(2)
P(2)–O(5)	1.514(2)	P(2)–O(6)	1.521(2)
P(2)–O(7)	1.535(2)	P(2)–O(8)	1.576(2)
N(1)–C(1)	1.343(4)	N(1)–C(5)	1.348(4)
N(2)–C(6)	1.348(4)	N(2)–C(10)	1.335(4)
C(1)–C(2)	1.379(4)	C(2)–C(3)	1.380(5)
C(3)–C(4)	1.383(5)	C(4)–C(5)	1.387(4)
C(5)–C(6)	1.480(4)	C(6)–C(7)	1.385(4)
C(7)–C(8)	1.387(5)	C(8)–C(9)	1.375(5)
C(9)–C(10)	1.381(4)	O(4)–H(4O)	0.826
O(8)–H(8O)	0.867	O(9)–H(9A)	0.908
O(9)–H(9B)	0.884		

[a] The C–H bond lengths are 0.93 Å.
[b] Symmetry codes: #1, $-x$, $-y+1$, $-z+1$; #2, $x+1$, y, z; #3, $-x$, $-y+2$, $-z+1$; #4, $-x-1$, $-y+2$, $-z+1$.

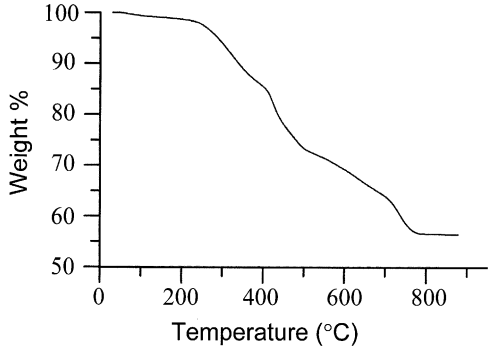

Fig. 2. The TG curve for **1** in flowing oxygen.

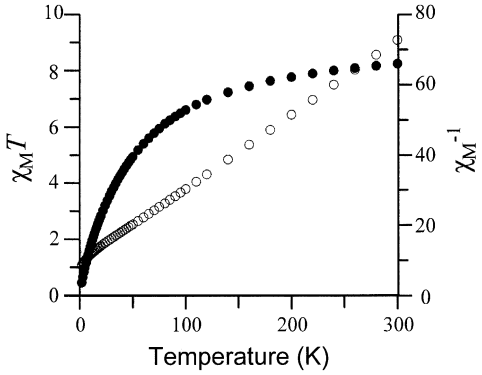

Fig. 3. $\chi_M T$ (solid circles) and χ_M^{-1} (open circles) plotted as a function of temperature for a powder sample of **1**.

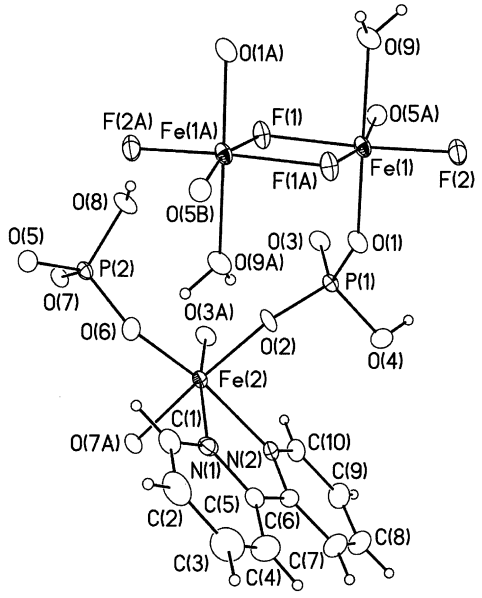

Fig. 4. The coordination environments of Fe atoms in the structure of **1** showing atom labeling scheme. Thermal ellipsoids are shown at 50% probability. Small open circles represent hydrogen atoms.

3.2. Crystal structure

The asymmetric unit consists of 27 unique non-hydrogen atoms. All atoms are at general positions. In the following only the structure of **1** will be discussed because the two compounds are isostructural. The local coordination environments of framework atoms in **1** are shown in Fig. 4. Both Fe(1) and Fe(2) are trivalent and are six-coordinate, however, they do not display the same coordination environment. Fe(1) is coordinated by two bridging F, one terminal F, one terminal water molecule and two HPO_4 ligands, while Fe(2) is coordinated by one bidendate 2,2′-bpy and four HPO_4 ligands. The three F atoms in $Fe(1)O_3F_3$ are in meridional configuration. An interesting structural feature of **1** is the presence of an edge-sharing dimer

formed of two $Fe(1)F_3O_3$ octahedra. Each dimer resides on an inversion center with two bridging F, two terminal F, two terminal water oxygen, and four phosphate oxygen atoms. A similar edge-sharing octahedral dimer with comparable Fe–F bond lengths has been observed in the fluorinated iron arsenate $(C_4H_{12}N_2)_{1.5}[Fe_3F_5(HAsO_4)_2(AsO_4)]$ [29]. The two distinct phosphorus atoms in **1** are tetrahedrally coordinated and are linked to one edge-shared dioctahedra and two discrete $Fe(2)O_4N_2$ octahedra through three oxygens to form two-dimensional neutral layers of fluorinated iron phosphate in the *ab* plane (Fig. 5a). The fourth coordination site in either phosphate corresponds to a terminal P–OH group. Consecutive layers are stacked one exactly above another so that infinite tunnels with four- and ten-membered rings are formed along the *c*-axis. As shown in Fig. 5b, each iron phosphate layer is decorated with 2,2′-bpy ligands projecting above and below into the interlamellar region. Neighboring 2,2′-bpy ligands from two adjacent layers have a structure of offset parallel stacking and are separated by 3.57 Å, indicating significant attractive intermolecular aromatic interaction. Thus, iron phosphate layers are extended into a three-dimensional supramolecular array via $\pi-\pi$ stacking interactions of the 2,2′-bpy ligands.

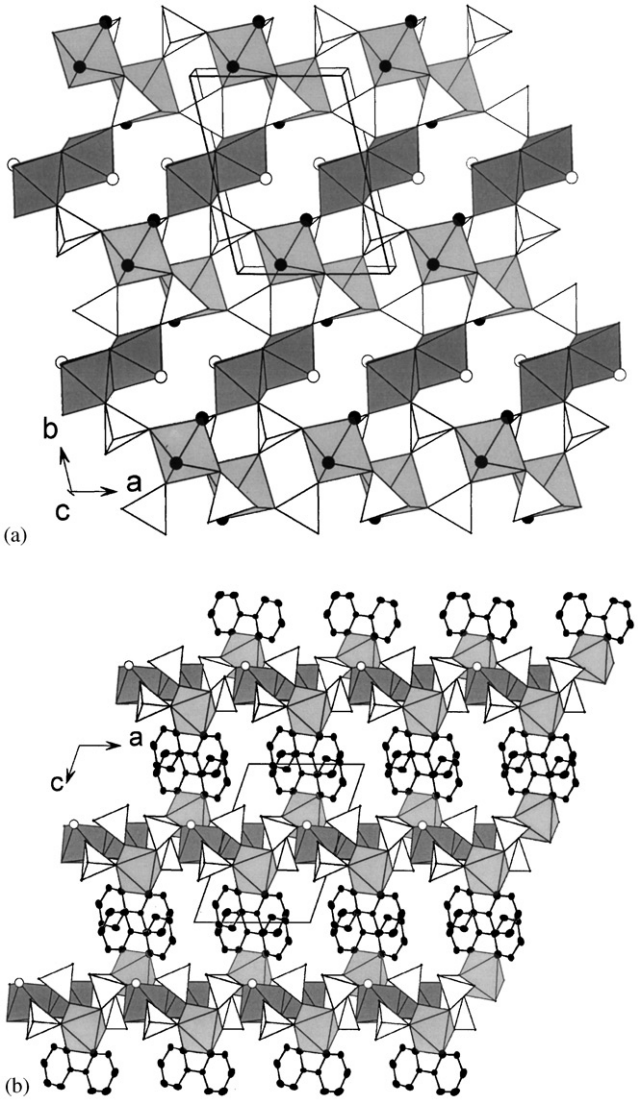

Fig. 5. (a) Section of an inorganic layer in **1** viewed along the *c*-axis. Edge-shared dioctahedra are shown in dark grey, FeO_4N_2 octahedra in light grey, and phosphate tetrahedral in white. Solid and open circles represent N and water O atoms, respectively. C and H atoms are not shown. (b) Structure of **1** viewed along the *b*-axis. Solid circles are C and N atoms. Open circles are water O atoms. H atoms are not shown.

Recently, Lu et al. reported a vanadium phosphate containing 2,2′-bpy ligand, $V_4O_7(HPO_4)_2(2,2'\text{-bpy})_2$ [30]. It also adopts a layer structure with the bidentate 2,2′-bpy ligands projecting into the interlamellar region. To our knowledge, this vanadium compound and $M_2F_2(2,2'\text{-bpy})(HPO_4)_2(H_2O)$ (M = Fe, Ga) are the only known examples in the 2,2′-bpy-phosphate system. Another two classes of hybrid compounds are based on oxalate-phosphate and 4,4′-bpy-phosphate. Metal phosphates containing organic components coordinated directly to metal atoms are scarce, as compared with the large number of metal phosphates in literature in which the organic components mostly occur as charge compensating and space-filling constituents. Given a variety of organic ligands that can be used in the synthesis, the scope for novel organic-inorganic hybrid metal phosphates appears to be very large. In a future publication we shall describe a layered metal phosphate incorporating a new organic ligand.

References

[1] R.C. Haushalter, L.A. Mundi, Chem. Mater. 4 (1992) 31 (and references therein).
[2] K.-H. Lii, Y.-F. Huang, V. Zima, C.-Y. Huang, H.-M. Lin, Y.-C. Jiang, F.-L. Liao, S.-L. Wang, Chem. Mater. 10 (1998) 2599 (and references therein).
[3] A.K. Cheetham, G. Férey, T. Loiseau, Angew. Chem. Int. Ed. 38 (1999) 3268 (and references therein).
[4] H.-M. Lin, K.-H. Lii, Y.-C. Jiang, S.-L. Wang, Chem. Mater. 11 (1999) 519.
[5] Z.A.D. Lethbridge, P. Lightfoot, J. Solid State Chem. 143 (1999) 58.
[6] A. Choudhury, S. Natarajan, C.N.R. Rao, J. Solid State Chem. 146 (1999) 538.
[7] A. Choudhury, S. Natarajan, J. Mater. Chem. 9 (1999) 3113.
[8] A. Choudhury, S. Natarajan, C.N.R. Rao, Chem.-A Eur. J. 6 (2000) 1168.
[9] W.-J. Chang, H.-M. Lin, K.-H. Lii, J. Solid State Chem. 157 (2000) 233.
[10] Y.-M. Tsai, S.-L. Wang, C.-H. Huang, K.-H. Lii, Inorg. Chem. 38 (1999) 4183.
[11] J. Do, R.P. Bontchev, A.J. Jacobson, Chem. Mater. 13 (2001) 2601.
[12] P. Lightfoot, Z.A.D. Lethbridge, R.E. Morris, D.S. Wragg, P.A. Wright, A. Kvick, G.B.M. Vaughan, J. Solid State Chem. 143 (1999) 74.

[13] C.-Y. Chen, P.P. Chu, K.-H. Lii, Chem. Commun. 16 (1999) 1473.
[14] K.-H. Lii, C.-Y. Chen, Inorg. Chem. 39 (2000) 3374.
[15] L.-C. Huang, H.-M. Kao, K.-H. Lii, Chem. Mater. 12 (2000) 2411.
[16] Y.-F. Huang, K.-H. Lii, J. Chem. Soc. Dalton Trans. 24 (1998) 4085.
[17] Z.A.D. Lethbridge, S.K. Tiwary, A. Harrison, P. Lightfoot, J. Chem. Soc. Dalton Trans. 12 (2001) 1904.
[18] K.-H. Lii, Y.-F. Huang, Inorg. Chem. 38 (1999) 1348.
[19] C.-Y. Chen, F.-R. Lo, H.-M. Kao, K.-H. Lii, Chem. Commun. 12 (2000) 1061.
[20] Y.-C. Jiang, Y.-C. Lai, S.-L. Wang, K.-H. Lii, Inorg. Chem. 40 (2001) 5320.
[21] L.-H. Huang, H.-M. Kao, K.-H. Lii, Inorg. Chem. 41 (2002) 2936.
[22] L.-I. Hung, S.-L. Wang, H.-M. Kao, K.-H. Lii, Inorg. Chem. 41 (2002) 3929.
[23] Z. Shi, S. Feng, S. Gao, L. Zhang, G. Yang, J. Hua, Angew. Chem. Int. Ed. 39 (2000) 2325.
[24] C.-M. Wang, K.-H. Lii, J. Solid State Chem., in press.
[25] M.I. Khan, J. Zubieta, Prog. Inorg. Chem. 34 (1995) 1.
[26] O. Kahn, Molecular Magnetism, VCH, New York, 1993.
[27] I.D. Brown, D. Altermatt, Acta Crystallogr. B 41 (1985) 244.
[28] G.M. Sheldrick, SHELXTL Programs, version 5.1, Bruker AXS GmbH, Karlsruhe, Germany, 1998.
[29] S.-H. Luo, Y.-C. Jiang, S.-L. Wang, H.-M. Kao, K.-H. Lii, Inorg. Chem. 40 (2001) 5381.
[30] Y. Lu, E. Wang, M. Yuan, G. Luan, Y. Li, H. Zhang, C. Hu, Y. Yao, Y. Qin, Y. Chen, J. Chem. Soc. Dalton Trans. 15 (2002) 3029.